Journal of Materials Chemistry A

ROYAL SOCIETY OF CHEMISTRY

PAPER

View Article Online
View Journal | View Issue

Cite this: J. Mater. Chem. A, 2023, 11, 21401

Simultaneous removal of C_2H_2 and C_2H_6 for C_2H_4 purification by robust MOFs featuring a high density of heteroatoms†

Shikai Xian,[ab] Junjie Peng,[c] Haardik Pandey,[d] Wells Graham,[d] Liang Yu,[c] Hao Wang,[a] Kui Tan,[e] Timo Thonhauser[d] and Jing Li*[ba]

Received 16th March 2023
Accepted 8th September 2023

DOI: 10.1039/d3ta01598j

rsc.li/materials-a

Simultaneous removal of C_2H_6 and C_2H_2 from C_2H_4 streams is of great importance in the petrochemical industry but remains a challenging task. To address this challenge, we have selected three isoreticular MOFs with high stability, low cost, and desirable scale-up ability, namely, MOF-303, MIL-160, and CAU-23 and assessed their potential in simultaneous removal of acetylene and ethane for ethylene purification. Each MOF exhibits desirable C_2H_2 and C_2H_6 uptake capacity (>5.5 mmol g^{-1} and >4 mmol g^{-1}, respectively), as well as good C_2H_2/C_2H_4 selectivity (>2) and C_2H_6/C_2H_4 selectivity (>1.5). Notably, MOF-303 takes up 4.96 mmol g^{-1} C_2H_6 at 298 K and 1 bar, the highest value among the three MOFs, with C_2H_6/C_2H_4 selectivity in the range of 1.55–2.47. MIL-160 possesses a very high C_2H_2 uptake (9.1 mmol g^{-1}) and C_2H_2/C_2H_4 selectivity, 10.6 (1 : 1, v/v), at 298 K, much higher than those of all other MOFs tested to date for simultaneous removal of C_2H_6 and C_2H_2 from C_2H_4. The results from breakthrough experiments confirm that all three MOFs demonstrate excellent performance for C_2H_4 purification in a ternary mixture of $C_2H_6/C_2H_4/C_2H_2$ (1 : 1 : 1, v/v/v). For MOF-303, MIL-160, and CAU-23, polymer-grade C_2H_4 up to 0.164, 0.21, and 0.181 mmol g^{-1} can be obtained from the equimolar ternary mixture in a single separation step from the breakthrough experiment. Additionally, DFT calculations have been performed to further investigate the mechanism of adsorption/separation for C_2H_6, C_2H_4, and C_2H_2.

1. Introduction

Ethylene (C_2H_4), one of the most important hydrocarbons used as feedstock to produce polyethylene, is generally produced from hydrocracking of fossil fuels.[1,2] During this process, two inevitable impurities, ethane (C_2H_6) and acetylene (C_2H_2), must be removed due to their harmful effect on the subsequent polyethylene production. C_2H_2 is poisonous to the catalyst of C_2H_4 polymerization, which dramatically reduces the quality of the resulting polyethylene.[3] On the other hand, the presence of even a small amount of C_2H_6 could lead to longer reaction times and a marked decrease in the efficiency of polyethylene production.[4] It is thus of great importance and necessity to remove C_2H_6 and C_2H_2 from C_2H_4 streams in order to produce high quality polyethylene. Partial hydrogenation and solvent extraction are the current commercial approaches for removal of C_2H_2, however, these approaches not only need noble metal catalysts and large amounts of organic solvent, but also require further purification of the C_2H_4 product to reach polymer grade.[5,6] For the removal of C_2H_6, current state-of-the-art strategies rely on cryogenic distillations that operate at high pressure and low temperature and suffer from high energy consumption and high installation costs of the separation units.[7,8]

As an alternative approach to cryogenic distillation, adsorptive separation using porous materials to purify C_2H_4 has demonstrated its eco-friendly and energy-efficient advantages.[9] Among diverse classes of porous materials, metal–organic frameworks (MOFs), constructed by metal clusters and organic linkers, are of particular interest owing to their advantageous features, such as extra-high surface area, structural tunability, linker tailorability, controllable properties, *etc.*[10] Recent studies have shown that MOFs exhibit superior separation performance for C_2H_4/C_2H_6 mixtures compared to traditional adsorbents such as zeolites.[11–14] However, for the vast majority of reported MOFs, especially those with open metal site (OMS) or π-complexation component, C_2H_4 is always preferentially adsorbed rather than C_2H_6, leading to not only substantial difficulty in obtaining high-purity C_2H_4 but also higher energy cost due to

[a]Hoffmann Institute of Advanced Materials, Shenzhen Polytechnic, 7098 Liuxian Boulevard, Shenzhen, Guangdong 518055, China
[b]Department of Chemistry and Chemical Biology, Rutgers University, 123 Bevier Road, Piscataway, New Jersey 08854, USA. E-mail: jingli@rutgers.edu
[c]School of Environmental and Chemical Engineering, Foshan University, 18 Jiangwan 1st Road, Chancheng, Foshan 528000, China
[d]Department of Physics, Center for Functional Materials, Wake Forest University, 1834 Wake Forest Road, Winston-Salem, North Carolina 27109, USA
[e]Department of Chemistry, University of North Texas, Denton, Texas 76201, USA

† Electronic supplementary information (ESI) available. See DOI: https://doi.org/10.1039/d3ta01598j

the more frequent adsorption–desorption switching.[4,15–17] Ideally, MOFs for C_2H_4/C_2H_6 separation should be based on an ethane selective mechanism because C_2H_6 is identified as an impurity with much lower quantities compared to C_2H_4. Thus, ethane-selective MOFs would achieve apparently reduced energy consumption along with greatly simplified separation operation and device. Current strategies for the development of ethane-selective materials mostly rely on strengthening van der Waals (VDWs) interactions between the hydrogen atoms of ethane and the heteroatoms of the organic linkers.[8,18–22] However, ethane-selective MOFs reported so far remain scarce, and their uptake capacity and selectivity are yet to be improved. Therefore, seeking for high-performance ethane-selective MOFs is an important task to be pursued. Similarly, removing C_2H_2 from C_2H_4 streams by using MOF adsorbents could become a promising alternative to current commercial approaches due to the lower energy cost and eco-friendly process.[23] Considering that ethane-selective MOFs can efficiently purify C_2H_4 by removing C_2H_6, and if choosing an ethane-selective MOF that can also selectively adsorb C_2H_2 over C_2H_4, simultaneous removal of C_2H_6 and C_2H_2 could be realized. Until now, only a few studies related to this approach have been reported,[4,5,23–25] and in all cases, while high purity C_2H_4 was produced in a single breakthrough experiment, there are some issues remaining to be resolved. For example, the working capacity of C_2H_6 and/or C_2H_2 is not high enough, leading to a low throughput efficiency of high-purity C_2H_4 with regard to time. On the other hand, several MOFs developed in these studies feature good C_2H_6/C_2H_4 selectivity but poor C_2H_2/C_2H_4 selectivity. For instance, according to the C_2H_2 breakthrough curves for NPU-1,[24] NPU-2,[24] and UPC-613,[25] the C_2H_2 breakthrough times are shorter than that of C_2H_6, namely, C_2H_2 would elute from the adsorbent bed before C_2H_6, resulting in a low yield of high-purity C_2H_4 in the simultaneous separation processes. Therefore, for simultaneous removal of C_2H_2 and C_2H_6, high C_2H_2 uptake capacity and selectivity are as important as high C_2H_6 uptake capacity and selectivity, which should be taken into consideration when developing new MOFs for this application. Generally, introducing OMS is an efficient strategy to design new MOFs with high C_2H_2 uptake and selectivity. However, this kind of MOF generally exhibits an ethylene selective feature owing to the stronger electrostatic interaction between OMS and C_2H_4 than between OMS and C_2H_6 (*e.g.*, Co-MOF-74,[26] Cu-BTC,[26] FJU-8 (ref. [27])), so simultaneous removal of C_2H_2 and C_2H_6 cannot be accomplished. Hence, it seems to be of great difficulty to achieve simultaneously high C_2H_6/C_2H_4 and C_2H_2/C_2H_4 selectivity as well as high C_2H_6 and C_2H_2 uptake. One possible solution is to include heteroatoms in the ligands. Several earlier reports have shown that these heteroatoms may serve as strong adsorption sites for C_2H_2 as a result of strong Lewis acid–base interaction between the Lewis basic site (heteroatom) and the acidic hydrogen atoms (at both ends of the C_2H_2 molecule).[27–30] Taking this into account, it is possible to obtain an ethane-selective MOF with high C_2H_2 uptake and selectivity by fine tuning the type and the amounts of heteroatoms, along with the pore structure.

Apart from separation performance, there are some other prerequisites that determine the feasibility for industrial applications, such as material cost, water/moisture stability and scale-up capability.[31] Stability, particularly water/moisture stability, is of great importance because it always determines the long-term storage/application and operational cost. Unfortunately, some ethane-selective MOFs such as $Ni(bdc)(ted)_{0.5}$ and IRMOF-8 feature high ethane uptake capacity but suffer from structural decomposition in humid air,[32] significantly lessening the feasibility of their application. On the other hand, while many other ethane-selective MOFs show sufficient water/moisture stability, such as PCN-250,[20] SNNU-40,[33] and CPM-733,[34] their ligands are quite expensive, which would seriously hinder their industrial application when considering the economic feasibility. In addition, some ethane-selective MOFs synthesized under relatively harsh conditions involving high temperature and pressure, large amounts of template reagents, or complex steps usually suffer from low scale-up ability because the total cost of instruments, chemicals, and energy would be extremely high for the scale up processes. Hence, in developing or selecting ethane-selective MOFs to be utilized in simultaneous removal of C_2H_2 and C_2H_6 for C_2H_4 purification, we must consider simultaneously all the factors and find an optimal balance between separation performance, stability, and cost.

In this work, we selected three highly stable Al-based MOFs, namely, MOF-303, MIL-160, and CAU-23, all of which feature similar 1D channels but different heteroatoms, as ethane-selective adsorbents to address the challenging task of simultaneous removal of C_2H_6 and C_2H_2 from C_2H_4 streams. All three Al-MOFs were synthesized following reported procedures with modifications.[35] Adsorption isotherms were measured by a volumetric method and used to calculate the corresponding ideal adsorbed solution theory (IAST) selectivity as well as the isosteric heats of adsorption. Ternary fixed bed breakthrough experiments were carried out to further confirm the potential for real-world applications. Finally, molecular simulations were performed to elucidate the adsorption mechanisms of C_2H_6, C_2H_4, and C_2H_2.

2. Materials and methods

2.1 Reagents and solvents

All reagents were purchased commercially and used as received. Aluminum chloride hexahydrate was purchased from Alfa Aesar; 3,5-pyrazoledicarboxylic acid monohydrate, 2,5-furandicarboxylic acid, and 2,5-thiophenedicarboxylic acid were all supplied by TCI America; sodium hydroxide was purchased from Acros Organics; the high-purity gases used in adsorption experiments were obtained from Praxair Inc. (New Jersey).

2.2 Preparation of MOF-303, MIL-160, and CAU-23

MOF-303 was prepared by using the procedure reported by Yaghi *et al.*[35] 1.04 g aluminum chloride hexahydrate ($AlCl_3 \cdot 6H_2O$, 4.308 mmol) and 0.75 g 3,5-pyrazoledicarboxylic acid monohydrate (H_3PDC, 4.308 mmol) were dissolved in 72 mL

water in a 200 mL glass flask, and 3 mL of aqueous NaOH (0.26 g, 6.5 mmol) were added dropwise to the above mixture under stirring. The flask was then heated at 100 °C with reflux for 12 h. After cooling down to room temperature, the as-synthesized MOF-303 powder was obtained by filtration. To remove the remaining 3,5-pyrazoledicarboxylic acid, the powder was washed thoroughly with water, followed by heating under vacuum at 150 °C for 12 h. MIL-160 and CAU-23 were obtained through the same process as that of MOF-303 by replacing the ligand 3,5-pyrazoledicarboxylic acid monohydrate with 2,5-furandicarboxylic acid and 2,5-thiophenedicarboxylic acid, respectively.

2.3 Characterization

Powder X-ray diffraction (PXRD) patterns were collected on an Ultima IV X-ray diffractometer in the scanning range of 3°–35° at 2.0 deg min^{-1}. Thermogravimetric analysis (TGA) was performed on a TA Q5000-IR analyzer, with temperature increased at a ramping rate of 10 K min^{-1} from ambient temperature to 973 K under a flowing nitrogen environment. Nitrogen adsorption isotherms were obtained at 77 K using a Micromeritics 3Flex analyzer. The BET model was chosen to evaluate the specific surface area, while the HK (Horvath–Kawazoe) method was applied to acquire the micropore size distribution.

2.4 Hydrocarbon adsorption experiments

C_2H_6, C_2H_4, and C_2H_2 sorption isotherms were recorded on the 3Flex analyzer. Volumetric sorption data were measured at various temperatures and pressures up to 1 bar. The desired temperature was controlled by employing a water bath (298–323 K) circulated by a precise temperature thermostat. Prior to data collection, 80–100 mg samples were degassed at 423 K for 12 h.

2.5 Breakthrough experiments

Breakthrough curves were obtained on a home-made experimental setup (Fig. S1†) at 298 K. Under the control of a mass flow meter, the velocity was set to be 1 mL min^{-1} for the ternary mixture $C_2H_6/C_2H_4/C_2H_2$ (1 : 1 : 1, v/v). A small-scale adsorption column was made by packing about 0.2 g of an activated sample into a long stainless hollow cylinder. The real time concentration of the effluent component was probed using a gas chromatography (GC) spectrometer (Agilent, 7890A). Before the experiment, the packed column was heated at 423 K under a 5 mL min^{-1} He flow for 1 h. After the breakthrough experiment, the desorption curves were measured at 298 K or 323 K under a 5 mL min^{-1} He flow.

2.6 Theoretical calculation method

All *ab initio* calculations were performed using density functional theory (DFT) in VASP (Vienna *Ab initio* Simulation Package),[36,37] with the vdW-DF functional[38–41] to take into account important van der Waals interactions. All the MOF unit cells were optimized by carrying out spin-polarized calculations, with SCF convergence of 0.1 meV and the plane wave energy cut-off set at 600 eV. The unit cell parameters and atoms were allowed to move till the force acting between atoms reached below 5 meV $Å^{-1}$. Potential binding sites were studied by placing C_2H_2, C_2H_4, and C_2H_6 molecules in MOF-303, MIL-160, and CAU-23 at various sites and all the atoms were allowed to relax in accordance with the convergence condition. The difference in the total energies of the MOF unit-cell and the guest molecules was used to calculate the corresponding binding energies. Induced charge densities were also calculated to map the variation in charge density upon introduction of the guest molecules and help identifying the interactions happening at the binding sites.

3. Results and discussion

3.1 Characterization

MOF-303, MIL-160, and CAU-23 are composed of infinite $Al(OH)(–COO)_2$ secondary building units (SBUs) linked through 3,5-pyrazoledicarboxylate, 2,5-furandicarboxylate, and 2,5-thiophenedicarboxylate, respectively. All three Al-MOFs feature 1D channels with small differences. As shown in Fig. 1(a), MOF-303 contains a straight channel because the SBUs are connected alternately by an equal number of *cis*- and *trans*-corner-sharing AlO_6 octahedra. The channel in CAU-23 is corrugated due to a large percent of *trans*- and small percent of *cis*-corner-sharing AlO_6 octahedra which form corresponding straight and helical sections in the infinite chain. For MIL-160, on the other hand, the SBUs are built only by *cis*-corner-sharing AlO_6 octahedra, forming a straight channel with alternate narrow and wide sections.

The sample purity of all three Al-MOFs was confirmed by powder X-ray diffraction (PXRD) analysis, and as shown in Fig. 1(c)–(e), the PXRD patterns of the as-synthesized MOFs match well with the corresponding simulated patterns. N_2 sorption experiments were conducted at 77 K to establish permanent microporosity of the MOFs. As expected, the three MOFs exhibit similar porosity due to their similar pore structure, with the BET surface areas of 1220 m^2 g^{-1}, 1188 m^2 g^{-1}, and 1242 m^2 g^{-1} for MOF-303, MIL-160, and CAU-23, respectively (Fig. S2–S4†), and pore sizes in the range of 5–7.5 Å (Fig. S5†). The high surface area and suitable pore size allow the channel to take up C_2H_6, C_2H_4, and C_2H_2 molecules with negligible diffusion hindrance. The thermal stability of the MOFs was evaluated by thermogravimetric (TG) analysis. As shown in Fig. 1(b), all three MOFs show two distinct weight loss steps: the first one before 125 °C corresponds to the weight loss of the solvent molecules, and the second one signifies the onset of framework decomposition beginning at 420 °C, 350 °C, and 380 °C for MOF-303, MIL-160, and CAU-23, respectively. Additionally, chemical stability was tested by comparing the PXRD patterns of samples before and after being treated under different conditions, including in boiling water for 24 h and in aqueous solutions with pH = 2 and pH = 12 for 24 h (Fig. 1(c)–(e)). The corresponding N_2 isotherms of the samples after being treated under different conditions were also measured at 77 K, and the results are plotted in Fig. S6.† As evident from these figures, both the PXRD patterns as well as the N_2 isotherms show no apparent changes in all

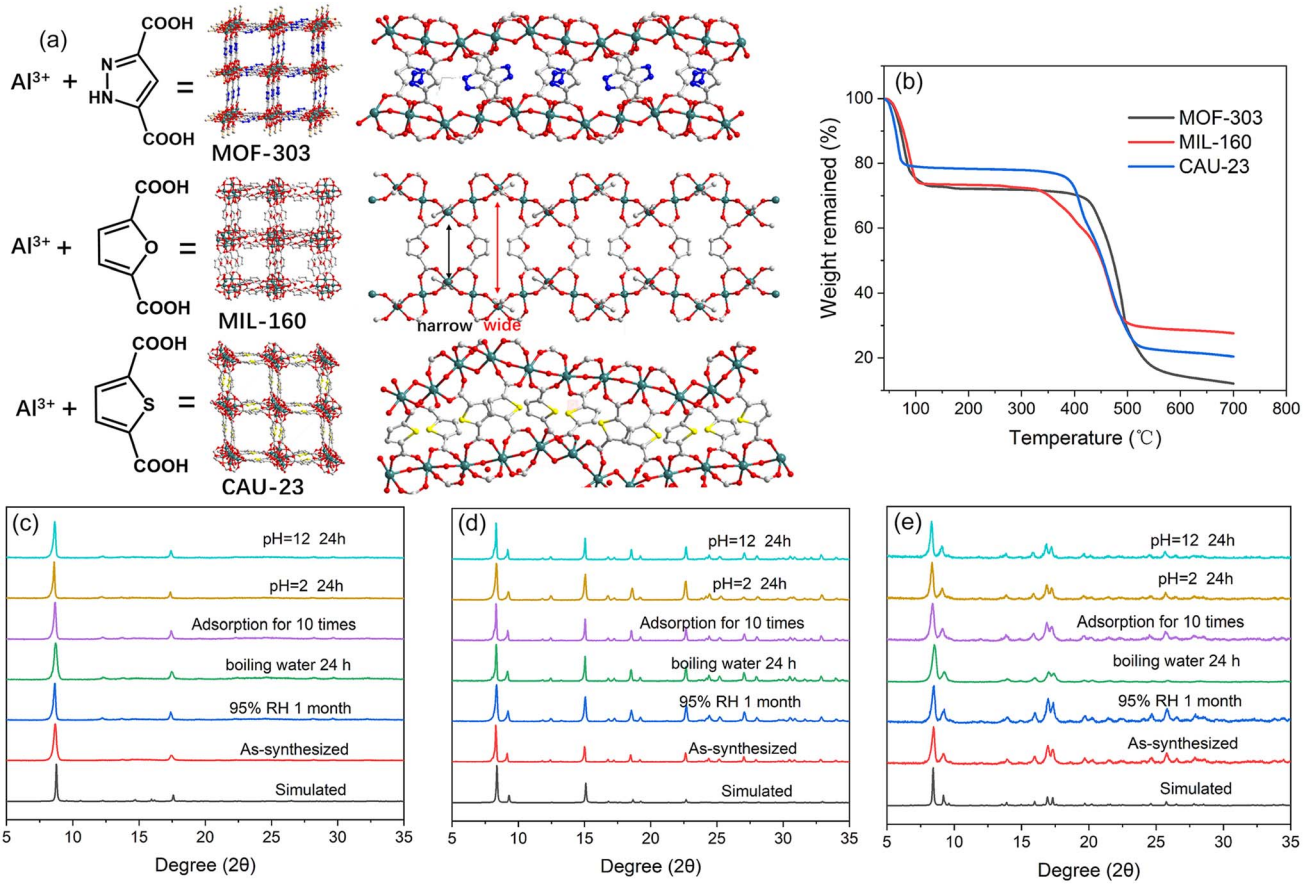

Fig. 1 (a) The composition and structure of MOF-303, MIL-160, and CAU-23 and the shape of pore windows and channels. (b) TG curves for MOF-303, MIL-160, and CAU-23. Simulated and experimental PXRD patterns of (c) MOF-303, (d) MIL-160, and (e) CAU-23 collected after their treatment under different conditions.

cases, revealing excellent structural stability of the three MOFs.

3.2 Single-component adsorption isotherms of C_2H_2, C_2H_4, and C_2H_6 and selectivity

The flourishing cavity, suitable pore size, and highly stable structure of these MOFs encouraged us to further investigate their performance in $C_2H_2/C_2H_4/C_2H_6$ separation. First, static adsorption, regarded as a highly effective approach to evaluate an adsorbent, was conducted upon MOF-303, MIL-160, and CAU-23. Adsorption isotherms of single component C_2H_6, C_2H_4, and C_2H_2 for the three MOFs were collected at 298 K, as presented in Fig. 2(a)–(c). In particular, all the C_2H_6 isotherms are type I with steep slopes, a typical feature of strong affinity towards adsorbates in microporous materials. The adsorbed amount of C_2H_6 is higher than that of C_2H_4 over the entire pressure range, indicating MOF-303, MIL-160, and CAU-23 are all ethane-selective. The C_2H_6 uptake capacity is of great importance for ethane-selective MOF as it is closely related to production output of pure C_2H_4 per unit time.[4] At 298 K and 1 bar, MOF-303, MIL-160, and CAU-23 adsorb 4.96, 4.65, and 4.30 mmol g^{-1} C_2H_6, respectively, which are higher than those of the majority of ethane-selective MOFs at the same conditions, such as $Fe_2(O_2)$(dobdc),[42] $Cu(Qc)_2$,[43] MAF-49,[8] *etc.* The value 4.96 mmol g^{-1} for MOF-303 is lower than those of SNNU-40 (7.54 mmol g^{-1}),[33] CPM-733 (7.13 mmol g^{-1}),[34] and CPM-233 (7.45 mmol g^{-1})[34] and slightly lower than those of Ni(bdc)$(ted)_{0.5}$ (5 mmol g^{-1})[44] and PCN-250 (5.21 mmol g^{-1}).[20] We also obtained simulated adsorption isotherms of both C_2H_4 and C_2H_6 at 298 K for all three MOFs (MOF-303, MIL-160, and CAU-23), which are generally consistent with the experimental data (Fig. S19–S21†). Compared to the C_2H_6 and C_2H_4 isotherms, C_2H_2 isotherms of all the three MOFs exhibit the highest uptake in the tested pressure range, as shown in Fig. 2(a)–(c), indicating the strongest interaction between C_2H_2 molecules and the frameworks. The adsorbed amounts for MOF-303 and CAU-23 are as high as 6.81 and 5.50 mmol g^{-1}, respectively, exceeding many other ethane-selective MOFs. Specifically, the C_2H_2 uptake of MIL-160 reaches 9.12 mmol g^{-1} at 298 K, much higher than those of other ethane-selective MOFs and comparable with those of MOFs with the highest acetylene uptakes, such as Co-MOF-74,[27] FJI-H8,[45] and ZJU-40a,[28] which possess open metal sites. The isosteric heats of adsorption were calculated for the three gases over the entire coverage range (Fig. S32†). For all three MOFs, the order was C_2H_2 > C_2H_6 > C_2H_4, well consistent with the isotherm data. Compared to MOF-303 and CAU-23, MIL-160 features the highest isosteric heats for all three gases, indicating the strongest interaction between the gas molecule and the framework, also consistent with

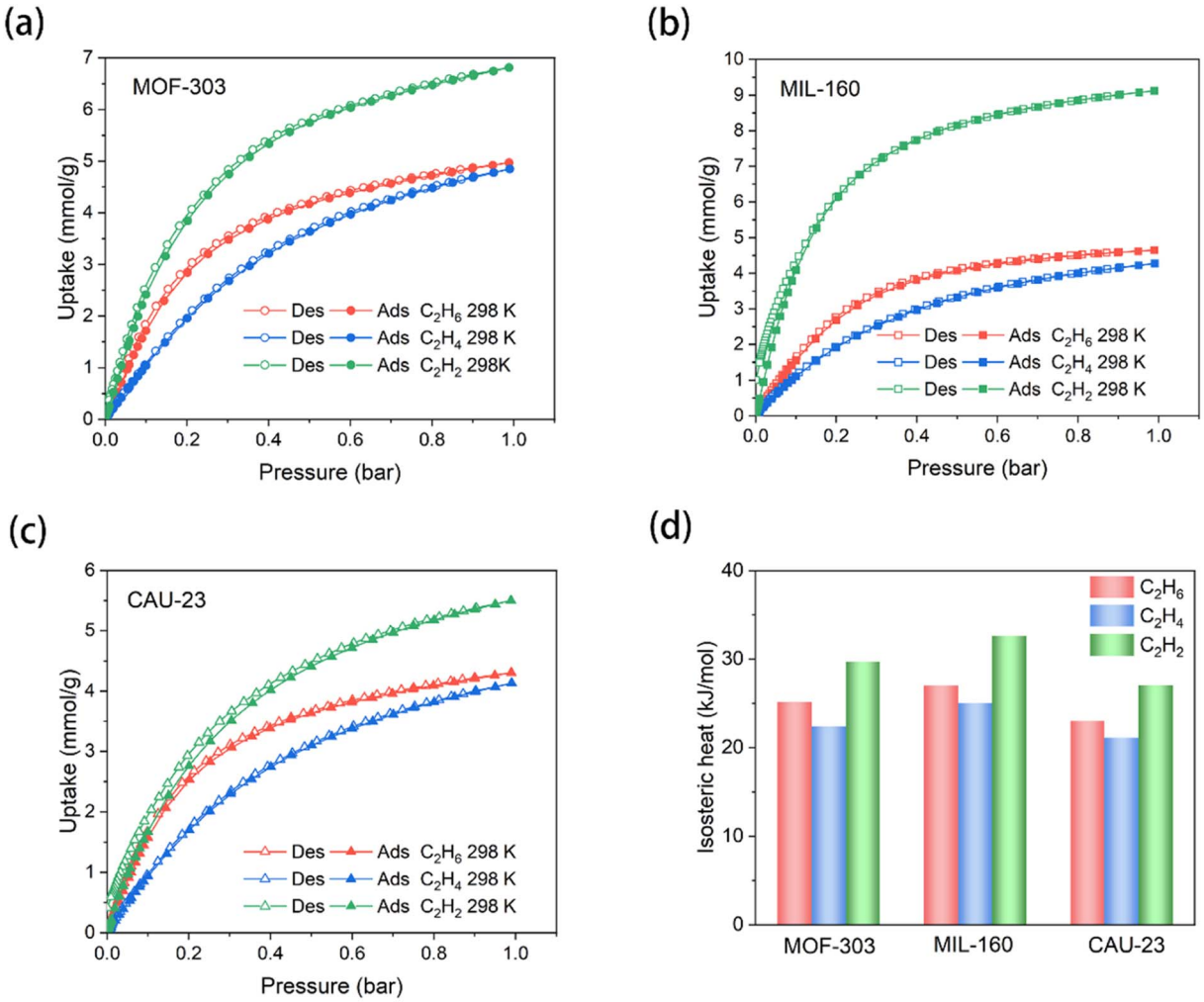

Fig. 2 C_2H_6, C_2H_4, and C_2H_2 adsorption–desorption isotherms of (a) MOF-303, (b) MIL-160, and (c) CAU-23 at 298 K. (d) Zero coverage isosteric heats for C_2H_6, C_2H_4, and C_2H_2 in MOF-303, MIL-160, and CAU-23.

the adsorption performance. The isosteric heats of C_2H_2 and C_2H_6 increase apparently with the coverage due to the strong H-bond between the C_2H_2 or C_2H_6 molecule. For C_2H_4, the enhancement is not as obvious, which could be attributed to the weaker interaction between the C_2H_4 and the framework. The data at zero coverage are shown in Fig. 2(d), where for C_2H_2 the values are 32.6 kJ mol^{-1} (MIL-160) > 29.7 kJ mol^{-1} (MOF-303) > 27.0 kJ mol^{-1} (CAU-23). For C_2H_6, a similar order is observed: 25.1 kJ mol^{-1} (MIL-160) > 22.4 kJ mol^{-1} (MOF-303) > 21.1 kJ mol^{-1} (CAU-23). For C_2H_4, as expected, the values are the lowest but also follow the same order: 28.32, 22.41, and 21.10 kJ mol^{-1} for MIL-160, MOF-303 and CAU-23, respectively. The order of isosteric heats may be ascribed to, at least partially, the different electronegativity of heteroatoms. For MIL-160, the O atom possesses the highest electronegativity leading to a strong C–H···O interaction, and the lower electronegativity of N and S gives rise to weaker interactions for MOF-303 and CAU-23.

It is noticed that although the ethane uptake amounts of PCN-250, CPM-733, CPM-233, and SNNU-40 are higher than those of MOF-303, MIL-160, and CAU-23 at 1 bar, the ligands of these MOFs are much more expensive than 3,5-pyrazoledicarboxylate, 2,5-furandicarboxylate, and 2,5-thiophenedicarboxylate in the title compounds, which would seriously hinder their industrial application when considering economic feasibility. Additionally, it has been verified that these three Al-based MOFs are very easy to scale up in water at 373 K within 24 h;[35] however, for PCN-250, CPM-733, CPM-233, and SNNU-40, the complex synthesis steps, higher temperature, and non-aqueous solvent may lead to an inevitable high cost for enlarging the production scale.

To further evaluate the separation properties of the three MOFs for the $C_2H_2/C_2H_6/C_2H_4$ mixture, IAST was employed to calculate the binary selectivities with the ratio of 1 : 1 (v/v, C_2H_6/C_2H_4 or C_2H_2/C_2H_4), and the results are shown in Fig. 3(a) and (b). The predicted selectivities of C_2H_6/C_2H_4 for MOF-303, MIL-160, and CAU-23 at 100 kPa are 1.55, 1.58, and 1.64, respectively, moderately high among the MOFs that have been tested for simultaneous removal of acetylene and ethane. For C_2H_2/C_2H_4, at 298 K and 100 kPa, while the values of MOF-303 and CAU-23 are already high, 2.59 and 2.06, respectively, the value for MIL-

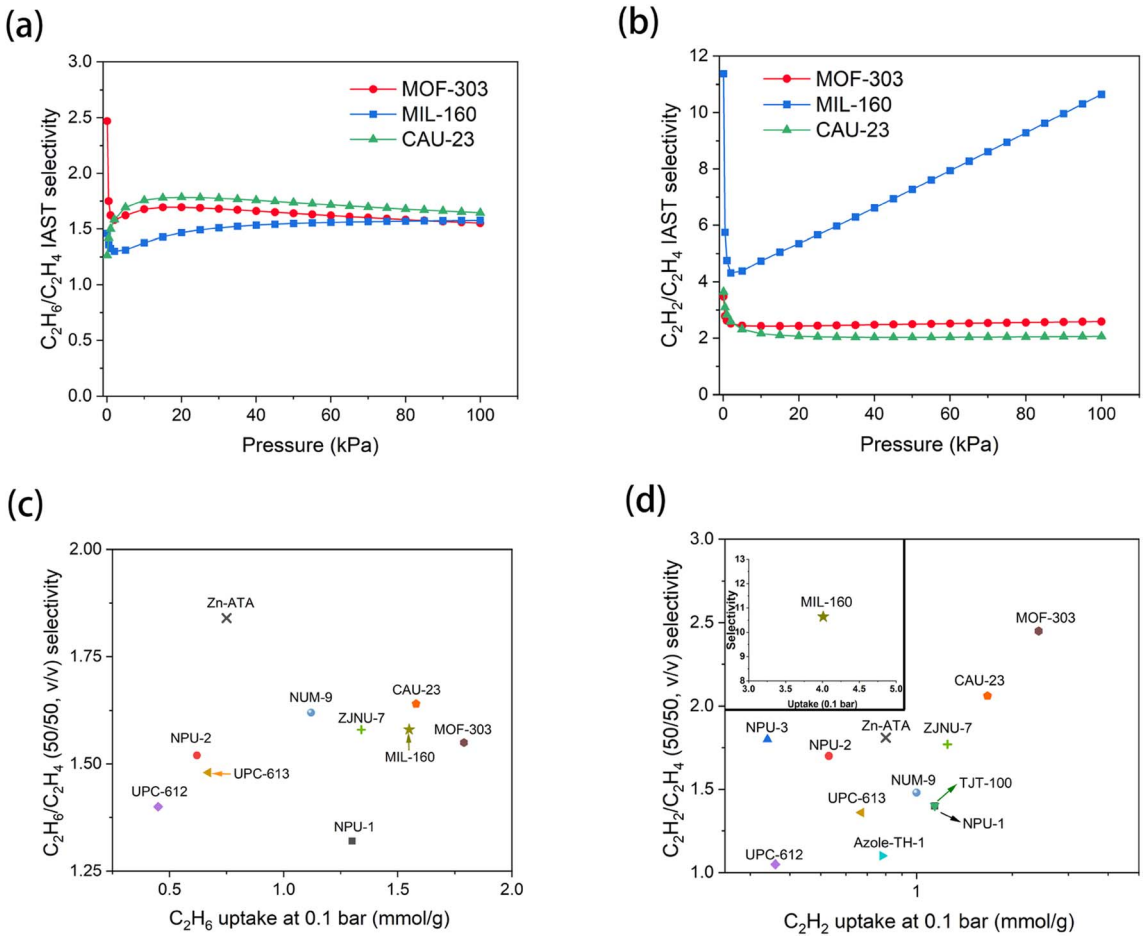

Fig. 3 IAST selectivity of (a) C_2H_6/C_2H_4 (1 : 1, v/v) and (b) C_2H_2/C_2H_4 (1 : 1, v/v) at 298 K for MOF-303, MIL-160, and CAU-23. Comparison of (c) C_2H_6/C_2H_4 selectivity (50/50, v/v) and C_2H_6 uptake at 298 K and 0.1 bar and (d) C_2H_2/C_2H_4 selectivity (50/50, v/v) and C_2H_2 uptake at 298 K and 0.1 bar between these three Al-MOFs and selected top-performing MOFs.

160 is 10.65, far surpassing MOF-303, CAU-23, and all the MOFs reported so far that have been evaluated for simultaneous removal of acetylene and ethane for ethylene purification. To intuitively assess the separation performance of MOF-303, MIL-160, and CAU-23, their uptake and selectivity values are compared with those of previously reported MOFs. Notably, the uptakes of C_2H_2 and C_2H_6 at 0.1 bar are chosen rather than those at 1 bar because the amounts of C_2H_2 and C_2H_6 in the gas mixtures after hydrocracking of fossil fuels are small, which is closer to reality. As shown in Fig. 3(c), the C_2H_6/C_2H_4 selectivities for MOF-303, MIL-160, and CAU-23 are lower than that for Zn-ATA, and comparable with those for NUM-9 and ZJNU-7 but higher than those for other MOFs. For C_2H_6 uptake at 298 K and 0.1 bar, MOF-303, CAU-23, and MIL-160 show a distinct advantage as their C_2H_6 uptake capacity is higher than that of all other MOFs, as shown in Fig. 3(c). For C_2H_2/C_2H_4 selectivity and C_2H_2 uptake at 0.1 bar, MOF-303 and CAU-23 apparently outstrip all the other MOFs except MIL-160. The C_2H_2/C_2H_4 selectivity and C_2H_2 uptake at 0.1 bar reach up to 10.64 and 4.01 mmol g^{-1}, respectively, as shown in Fig. 3(d). The appreciable C_2H_2 uptake, along with the high C_2H_2/C_2H_4 selectivity and C_2H_2 isosteric heat may be attributed to the specific base–acid specific interaction between the two acidic hydrogen atoms at both ends of C_2H_2 and the high density of Lewis basic heteroatom sites fully exposed on the surface of the 1D channel, forming strong H–C≡C–H···M (heteroatom in the ligands) hydrogen bonding.[28] The competitive selectivity for C_2H_2/C_2H_4 and C_2H_6/C_2H_4 along with the high uptake of C_2H_2 and C_2H_6 at low pressure demonstrate exceedingly high performance in simultaneous removal of acetylene and ethane for ethylene purification.

3.3 Theoretical calculations

To understand the mechanism of C_2 hydrocarbon adsorption on MOF-303, MIL-160, and CAU-23, density functional theory (DFT) calculations were performed. Fig. 4(a)–(c) show that the primary binding sites of C_2H_2, C_2H_4 and C_2H_6 are near the MOF linkers. The strongest interaction occurs with C_2H_2 and a binding energy of 97.6 kJ mol^{-1} was obtained. The binding energy of C_2H_6 was calculated to be 80.0 kJ mol^{-1}, larger than that of C_2H_4 (74.6 kJ mol^{-1}). The order of the binding energies (C_2H_2 > C_2H_6 > C_2H_4) coincides well with the experimental results, such as the zero coverage isosteric heats and the uptakes. As shown in Fig. 4(a), C_2H_2 interacts strongly with

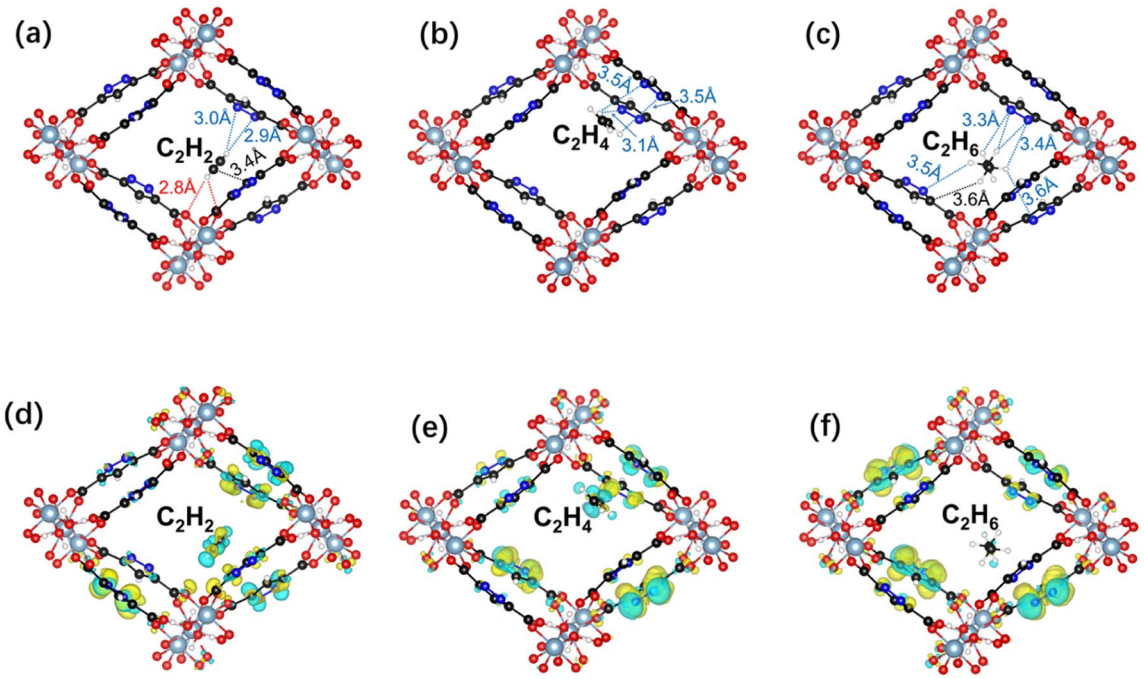

Fig. 4 The primary binding sites in the MOF-303 structure for (a) C_2H_2, (b) C_2H_4, and (c) C_2H_6. Induced charge densities for (d) C_2H_2, (e) C_2H_4, and (f) C_2H_6, with an iso-level of 0.001 electrons per Å^3. The blue highlights represent the decrease in charge and yellow highlights show the increase in charge after binding of the molecules.

multiple linkers through N and O atoms. The induced charge densities plotted in Fig. 4(d) show that the interaction with the linker rings is primarily *via* π-bonds, where N atoms, located at a short distance from the acetylene, act as stronger adsorption sites compared to the C atoms. The results also point towards a H-bond type interaction with the O atoms from the COO^- group (present at the metal cluster), resulting in a high binding energy for C_2H_2. In the case of C_2H_4, the molecule also interacts with linker rings but at longer distances (Fig. 4(b)), with the interaction concentrated at the C–H bonds (as shown by the induced charge densities, Fig. 4(e)), indicative of a much weaker binding strength. The C_2H_6 molecule at its primary binding site is shifted more towards the center of the pore due to its larger kinetic diameter (Fig. 4(c)). However, the induced charge densities in Fig. 4(f) show that C_2H_6 interacts mainly with the N atoms of the linkers *via* C–H bonds, and the number of linkers involved in the interaction is higher than that of C_2H_4, resulting in a stronger interaction and higher binding energy. The binding energy calculations for MIL-160 showcase the binding strength order of C_2H_2 (52.3 kJ mol^{-1}) > C_2H_6 (50.9 kJ mol^{-1}) > C_2H_4 (46.2 kJ mol^{-1}), when binding at the primary binding site (Fig. S16†). The induced charge densities, representing the redistribution of charge on binding, are also shown in Fig. S16.† All three guest molecules prefer binding near the linkers, interacting primarily with the O atoms that are part of the linkers *via* their C–H bonds. The binding energy calculations for CAU-23 showcase the same trend as in the case of MIL-160, with the binding energy of C_2H_2 (44.4 kJ mol^{-1}) > C_2H_6 (40.2 kJ mol^{-1}) > C_2H_4 (34.1 kJ mol^{-1}), at their primary binding sites located near the MOF linker (Fig. S17†). The induced charge densities, representing the redistribution of charge on binding, are also shown in Fig. S17.† Similar to the case for MIL-160, all three guest molecules have their primary binding site at the linkers, interacting primarily with the S atoms that are part of the linkers *via* their C–H bonds. The C_2H_6 molecule also has additional strong interaction with the O–H group at the metal cluster contributing to its larger binding energy.

3.4 Breakthrough experiments and regeneration tests

To evaluate the separation potential of MOF-303, MIL-160, and CAU-23 under conditions similar to the industrial settings, dynamic breakthrough experiments were carried out on ternary ($C_2H_6/C_2H_4/C_2H_2$, 1 : 1 : 1, v/v/v) gas mixtures. As shown in Fig. 5(a), C_2H_4 eluted out first at 14.8 min, followed by C_2H_6 and C_2H_2 with a breakthrough time of 17 and 20.6 min, respectively, coinciding well with the isosteric heats and the theoretical calculation results. The relatively short intervals between the breakthrough times for C_2H_4 and C_2H_6 are attributed to their similar isosteric heats and binding energies, and for C_2H_2, the higher isosteric heat and binding energy are responsible for the longer breakthrough time. In Fig. 5(b) and (c), similar curves with different breakthrough times were observed. The breakthrough time of MIL-160 for C_2H_2 is more than 30 min, much longer than that of MOF-303 and CAU-23, consistent with the high C_2H_2 uptake and C_2H_2/C_2H_4 selectivity. As expected, the breakthrough times of CAU-23 for C_2H_2, C_2H_6, and C_2H_4 are the shortest among the three MOFs. In Fig. 5(a), before the breakthrough of C_2H_6, C_2H_4 of polymer-grade purity (>99.9%) can be harvested, with a productivity of 0.164 mmol g^{-1}, confirming the ability of MOF-303 to produce polymer-grade C_2H_4 from 1 :

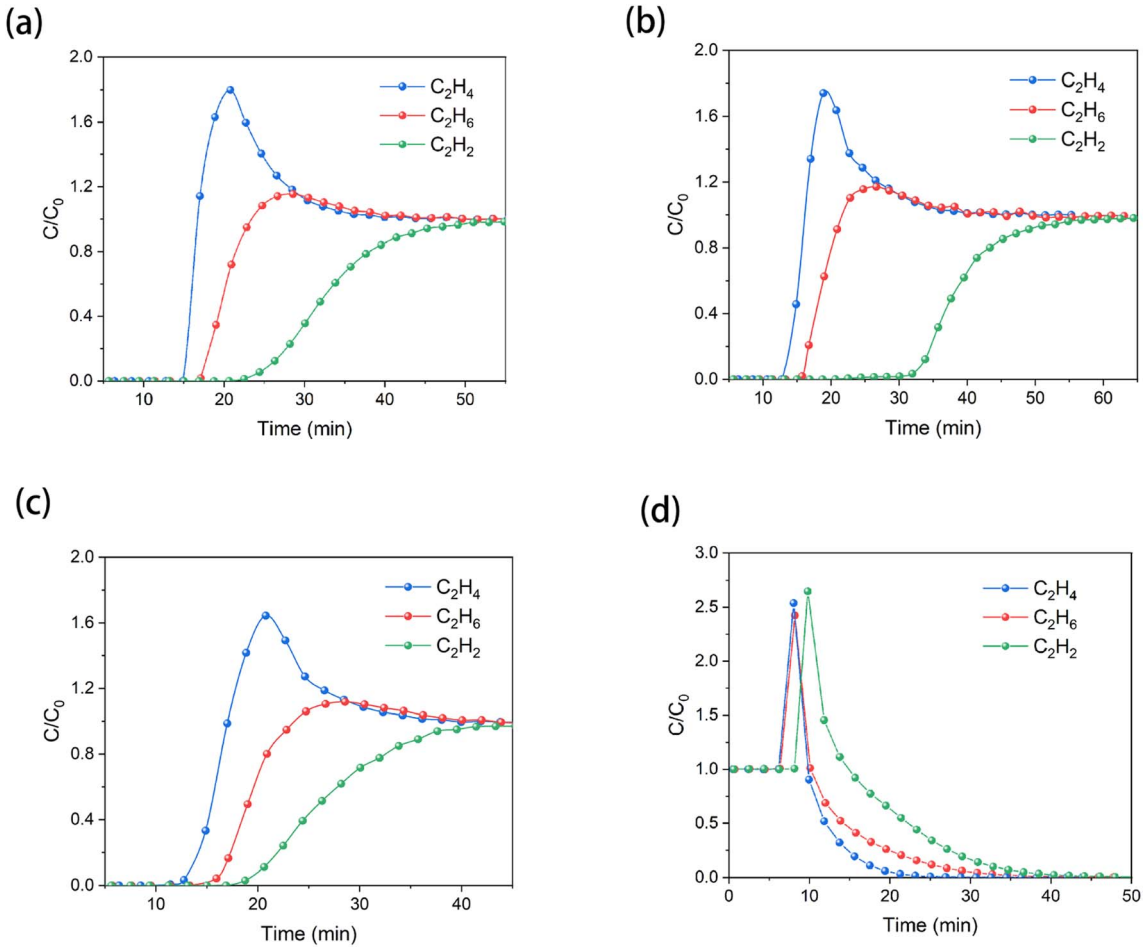

Fig. 5 Dynamic breakthrough curves for a ternary gas mixture ($C_2H_6/C_2H_4/C_2H_2$, 1 : 1 : 1, v/v/v) on (a) MOF-303, (b) MIL-160, and (c) CAU-23 at 298 K and 100 kPa. (d) Desorption curves for the MOF-303 packed column at 323 K under a 5 mL min^{-1} He flow.

1 : 1 $C_2H_2/C_2H_4/C_2H_6$ in a single separation step. For MIL-160 and CAU-23, the productivity values are 0.21 and 0.181 mmol g^{-1}, respectively. For C_2H_4 productivity, MIL-160 is only comparable with MOF-303 and CAU-23 although its C_2H_2 uptake capacity and C_2H_2/CH_4 selectivity are impressive, which may be due to the similar C_2H_6/C_2H_4 selectivity among the three MOFs. In addition, owing to the strong affinity of C_2H_2, competitive adsorption between C_2H_2 and C_2H_6 molecules in MIL-160 may sharply shorten the C_2H_6 breakthrough time, leading to a reduced productivity of high-purity C_2H_4. The productivity of the three Al-MOFs greatly exceeds that of NPU-1 (0.075 mmol g^{-1}) and NPU-2 (~0.01 mmol g^{-1})[24] but is less than that of UPC-612 (0.47 mmol g^{-1}) and UPC-613 (0.34 mmol g^{-1})[25] under the same experimental conditions. Although the C_2H_4 productivity of UPC-612 is more than twice the amount of the three Al-MOFs, considering that the synthesis of TCBCBCPC, the ligand of UPC-612, is very complex and even the starting materials of TCBCBCPC are much more expensive than the ligands in MOF-303, MIL-160, and CAU-23, the latter group is much more suitable for industrial applications.

To evaluate the regeneration performance of MOF-303, MIL-160, and CAU-23, desorption curves were recorded at low-cost conditions, 323 K and 5 mL min^{-1} He flow, after a single separation step. As shown in Fig. 5(d), during the desorption process of MOF-303, C_2H_4, C_2H_6, and C_2H_2 can be fully removed in 28, 40, and 50 min, respectively, demonstrating that the MOF-303 column can be fully activated by heating at 323 K for 50 min. For MIL-160 and CAU-23, the fully active times are 65 and 40 min, as shown in Fig. S25 and S26,† which suggests that CAU-23 is more promising when used for simultaneous removal of acetylene and ethane for ethylene purification compared to MOF-303 because of the higher polymer-grade C_2H_4 productivity and the lower regeneration energy cost. Finally, binary gas mixture breakthrough experiments were also conducted for another 4 adsorption–desorption cycles consecutively to further test the recycling performance of MOF-303, MIL-160, and CAU-23. As illustrated in Fig. S27–S29,† the breakthrough time for C_2H_4 remains nearly constant, consistent with the results of 10 continuous C_2H_6 adsorption–desorption cycles on all three MOFs measured at 298 K (Fig. S30†). These results provide solid evidence of the excellent stability of the three MOFs.

To evaluate how water molecules may affect the purification of ethylene, we further carried out breakthrough experiments for a ternary gas mixture ($C_2H_6/C_2H_4/C_2H_2$, 1 : 1 : 1, v/v/v) on

MOF-303 under 45% RH, as shown in Fig. S31.† Except for the humidity, other experimental conditions are the same as the conditions shown in Section 2.5 in the manuscript. Compared with the separation under dry conditions, the three gases follow the same breakout order, but with decreased breakthrough times, owning to the competitive water adsorption (Table S11†). We found the duration between the C_2H_4 and C_2H_6 breakthrough that determines the yield of high purity ethylene under 45% RH is 182 s, nearly the same as that under dry conditions, 180 s, suggesting that 45% RH has no effect on the yield of high purity ethylene, although the uptake of C_2H_4, C_2H_6, and C_2H_2 is reduced by the competitive adsorption of water. Similarly, the yield of high purity ethylene for MIL-160 and CAU-23 may not be affected by water vapour, but the adsorbed amounts would be decrease remarkably due to the hydrophilic frameworks. These results further confirm that MOF-303, MIL-160, and CAU-23 are promising adsorbents for simultaneous removal of C_2H_6 and C_2H_2 from C_2H_4 streams.

4. Conclusion

Three highly stable Al-based MOFs, MOF-303, MIL-160, and CAU-23, were investigated for C2 hydrocarbon separations. All three ethane-selective MOFs show high C_2H_6 uptake and good C_2H_6/C_2H_4 selectivity. Notably, the C_2H_6 uptakes in MOF-303, MIL-160 and CAU-23 reach up to 4.96, 4.65, and 4.3 mmol g^{-1} at 298 K and 1 bar, outperforming most ethane-selective MOFs reported to date. Taking into consideration their ultrahigh C_2H_2 adsorption capacity at low pressure (*e.g.*, 0.1 bar), 2.42 mmol g^{-1} for MOF-303, 4.01 mmol g^{-1} for MIL-160, and 1.67 mmol g^{-1} for CAU-23, and excellent C_2H_2/C_2H_4 selectivity, 2.45, 10.46, and 2.06, respectively, we further assessed their ability to simultaneously remove C_2H_6 and C_2H_2 from C_2H_4. Our results from breakthrough experiments on these Al-MOFs show that polymer-grade high-purity C_2H_4 can be achieved in one step from a ternary mixture of $C_2H_2/C_2H_4/C_2H_6$, with a productivity of 0.164, 0.21, and 0.181 mmol g^{-1}, respectively for MOF-303, MIL-160, and CAU-23, higher than some of the best-performing MOFs, such as NPU-1 and NPU-2. The MOF-filled columns can be fully activated/regenerated at moderate temperature (50 °C or 323 K) in less than 65 min, and no sign of degradation was detected in four cycles. DFT calculations reveal that the strong affinity between C_2H_6 (or C_2H_2) and the heteroatom of the linker molecules gives rise to the high loading capacity and selectivity for C_2H_2 and C_2H_6. Overall, the three Al-based MOFs, MOF-303, MIL-160, and CAU-23, represent promising candidates for industrial adsorptive C_2H_4 purification with a good balance between stability, cost, and performance.

Conflicts of interest

There are no conflicts to declare.

Acknowledgements

We would like to thank the U. S. Department of Energy, Office of Science, Office of Basic Energy Sciences (Grant No. DE-SC0019902) for the partial support of this work. S. Xian, J. Peng and H. Wang acknowledge the financial support from the National Natural Science Foundation of China (No. 21908069, 21901166), Guangdong Natural Science Foundation (2019A1515010692), and Shenzhen Science and Technology Program (No. JCYJ20190809145615620, RCYX20200714114539243).

References

1 I. Amghizar, L. A. Vandewalle, K. M. Van Geem and G. B. Marin, *Engineering*, 2017, **3**, 171–178.
2 Y. He, R. Krishna and B. Chen, *Energy Environ. Sci.*, 2012, **5**, 9107–9120.
3 H. Molero, B. F. Bartlett and W. T. Tysoe, *J. Catal.*, 1999, **181**, 49–56.
4 H.-G. Hao, Y.-F. Zhao, D.-M. Chen, J.-M. Yu, K. Tan, S. Ma, Y. Chabal, Z.-M. Zhang, J.-M. Dou, Z.-H. Xiao, G. Day, H.-C. Zhou and T.-B. Lu, *Angew. Chem., Int. Ed.*, 2018, **57**, 16067–16071.
5 Z. Xu, X. Xiong, J. Xiong, R. Krishna, L. Li, Y. Fan, F. Luo and B. Chen, *Nat. Commun.*, 2020, **11**, 3163.
6 B. Wang, L.-H. Xie, X. Wang, X.-M. Liu, J. Li and J.-R. Li, *Green Energy Environ.*, 2018, **3**, 191–228.
7 O. T. Qazvini, R. Babarao, Z.-L. Shi, Y.-B. Zhang and S. G. Telfer, *J. Am. Chem. Soc.*, 2019, **141**, 5014–5020.
8 P.-Q. Liao, W.-X. Zhang, J.-P. Zhang and X.-M. Chen, *Nat. Commun.*, 2015, **6**, 8697.
9 W.-G. Cui, T.-L. Hu and X.-H. Bu, *Adv. Mater.*, 2020, **32**, 1806445.
10 J.-R. Li, J. Yu, W. Lu, L.-B. Sun, J. Sculley, P. B. Balbuena and H.-C. Zhou, *Nat. Commun.*, 2013, **4**, 1538.
11 R.-B. Lin, L. Li, H.-L. Zhou, H. Wu, C. He, S. Li, R. Krishna, J. Li, W. Zhou and B. Chen, *Nat. Mater.*, 2018, **17**, 1128–1133.
12 S. Yang, A. J. Ramirez-Cuesta, R. Newby, V. Garcia-Sakai, P. Manuel, S. K. Callear, S. I. Campbell, C. C. Tang and M. Schröder, *Nat. Chem.*, 2015, **7**, 121–129.
13 P. Verma, X. Xu and D. G. Truhlar, *J. Phys. Chem. C*, 2013, **117**, 12648–12660.
14 X. Wang, Y. Wu, J. Peng, Y. Wu, J. Xiao, Q. Xia and Z. Li, *Chem. Eng. J.*, 2019, **358**, 1114–1125.
15 Y. Chang, H. Huang, H. Zhu, Y. Zhao, L. Wang, Y. Sun and C. Zhong, *Chem. Eng. J.*, 2022, **427**, 131726.
16 S. J. Geier, J. A. Mason, E. D. Bloch, W. L. Queen, M. R. Hudson, C. M. Brown and J. R. Long, *Chem. Sci.*, 2013, **4**, 2054–2061.
17 S. Horike, Y. Inubushi, T. Hori, T. Fukushima and S. Kitagawa, *Chem. Sci.*, 2012, **3**, 116–120.
18 D.-L. Chen, N. Wang, C. Xu, G. Tu, W. Zhu and R. Krishna, *Microporous Mesoporous Mater.*, 2015, **208**, 55–65.
19 D. Lv, R. Shi, Y. Chen, Y. Wu, H. Wu, H. Xi, Q. Xia and Z. Li, *ACS Appl. Mater. Interfaces*, 2018, **10**, 8366–8373.
20 Y. Chen, Z. Qiao, H. Wu, D. Lv, R. Shi, Q. Xia, J. Zhou and Z. Li, *Chem. Eng. Sci.*, 2018, **175**, 110–117.
21 S. Geng, E. Lin, X. Li, W. Liu, T. Wang, Z. Wang, D. Sensharma, S. Darwish, Y. H. Andaloussi, T. Pham, P. Cheng, M. J. Zaworotko, Y. Chen and Z. Zhang, *J. Am. Chem. Soc.*, 2021, **143**, 8654–8660.

22 L. Yang, Y. Wang, Y. Chen, J. Yang, X. Wang, L. Li and J. Li, *Chem. Eng. J.*, 2020, **387**, 124137.
23 T.-L. Hu, H. Wang, B. Li, R. Krishna, H. Wu, W. Zhou, Y. Zhao, Y. Han, X. Wang, W. Zhu, Z. Yao, S. Xiang and B. Chen, *Nat. Commun.*, 2015, **6**, 7328.
24 B. Zhu, J.-W. Cao, S. Mukherjee, T. Pham, T. Zhang, T. Wang, X. Jiang, K. A. Forrest, M. J. Zaworotko and K.-J. Chen, *J. Am. Chem. Soc.*, 2021, **143**, 1485–1492.
25 Y. Wang, C. Hao, W. Fan, M. Fu, X. Wang, Z. Wang, L. Zhu, Y. Li, X. Lu, F. Dai, Z. Kang, R. Wang, W. Guo, S. Hu and D. Sun, *Angew. Chem., Int. Ed.*, 2021, **60**, 11350–11358.
26 S. Xiang, W. Zhou, J. M. Gallegos, Y. Liu and B. Chen, *J. Am. Chem. Soc.*, 2009, **131**, 12415–12419.
27 J. Pang, F. Jiang, M. Wu, C. Liu, K. Su, W. Lu, D. Yuan and M. Hong, *Nat. Commun.*, 2015, **6**, 7575.
28 H.-M. Wen, H. Wang, B. Li, Y. Cui, H. Wang, G. Qian and B. Chen, *Inorg. Chem.*, 2016, **55**, 7214–7218.
29 T. Ke, Q. Wang, J. Shen, J. Zhou, Z. Bao, Q. Yang and Q. Ren, *Angew. Chem., Int. Ed.*, 2020, **59**, 12725–12730.
30 R.-B. Lin, L. Li, H. Wu, H. Arman, B. Li, R.-G. Lin, W. Zhou and B. Chen, *J. Am. Chem. Soc.*, 2017, **139**, 8022–8028.
31 X.-J. Kong and J.-R. Li, *Engineering*, 2021, **7**, 1115–1139.
32 D. Lv, J. Chen, Y. Chen, Z. Liu, Y. Xu, C. Duan, H. Wu, Y. Wu, J. Xiao, H. Xi, Z. Li and Q. Xia, *AIChE J.*, 2019, **65**, e16616.
33 A. N. Hong, H. Yang, T. Li, Y. Wang, Y. Wang, X. Jia, A. Zhou, E. Kusumoputro, J. Li, X. Bu and P. Feng, *ACS Appl. Mater. Interfaces*, 2021, **13**, 52160–52166.
34 H. Yang, Y. Wang, R. Krishna, X. Jia, Y. Wang, A. N. Hong, C. Dang, H. E. Castillo, X. Bu and P. Feng, *J. Am. Chem. Soc.*, 2020, **142**, 2222–2227.
35 F. Fathieh, M. J. Kalmutzki, E. A. Kapustin, P. J. Waller, J. Yang and O. M. Yaghi, *Sci. Adv.*, 2018, **4**, eaat3198.
36 G. Kresse and J. Furthmüller, *Phys. Rev. B: Condens. Matter Mater. Phys.*, 1996, **54**, 11169–11186.
37 G. Kresse and D. Joubert, *Phys. Rev. B: Condens. Matter Mater. Phys.*, 1999, **59**, 1758–1775.
38 K. Berland, V. R. Cooper, K. Lee, E. Schröder, T. Thonhauser, P. Hyldgaard and B. I. Lundqvist, *Rep. Prog. Phys.*, 2015, **78**, 066501.
39 D. C. Langreth, B. I. Lundqvist, S. D. Chakarova-Käck, V. R. Cooper, M. Dion, P. Hyldgaard, A. Kelkkanen, J. Kleis, L. Kong, S. Li, P. G. Moses, E. Murray, A. Puzder, H. Rydberg, E. Schröder and T. Thonhauser, *J. Phys.: Condens. Matter*, 2009, **21**, 084203.
40 T. Thonhauser, V. R. Cooper, S. Li, A. Puzder, P. Hyldgaard and D. C. Langreth, *Phys. Rev. B: Condens. Matter Mater. Phys.*, 2007, **76**, 125112.
41 T. Thonhauser, S. Zuluaga, C. A. Arter, K. Berland, E. Schröder and P. Hyldgaard, *Phys. Rev. Lett.*, 2015, **115**, 136402.
42 L. Li, R.-B. Lin, R. Krishna, H. Li, S. Xiang, H. Wu, J. Li, W. Zhou and B. Chen, *Science*, 2018, **362**, 443.
43 R.-B. Lin, H. Wu, L. Li, X.-L. Tang, Z. Li, J. Gao, H. Cui, W. Zhou and B. Chen, *J. Am. Chem. Soc.*, 2018, **140**, 12940–12946.
44 W. Liang, F. Xu, X. Zhou, J. Xiao, Q. Xia, Y. Li and Z. Li, *Chem. Eng. Sci.*, 2016, **148**, 275–281.
45 S. Xiang, W. Zhou, Z. Zhang, M. A. Green, Y. Liu and B. Chen, *Angew. Chem., Int. Ed.*, 2010, **49**, 4615–4618.